Structure of mitochondrial ADP/ATP carrier in complex with carboxyatractyloside

Eva Pebay-Peyroula[1], Cécile Dahout-Gonzalez[2], Richard Kahn[1], Véronique Trézéguet[3], Guy J.-M. Lauquin[3] & Gérard Brandolin[2]

[1]*Institut de Biologie Structurale, UMR 5075 CEA-CNRS-Université Joseph Fourier, 41 rue Jules Horowitz, F-38027, Grenoble cedex 1, France*
[2]*Laboratoire de Biochimie et Biophysique des Systèmes Intégrés, UMR 5092 CEA-CNRS-Université Joseph Fourier, Département de Réponse et Dynamique Cellulaires, CEA-Grenoble, 17 Avenue des Martyrs, F-38054 Grenoble cedex 9, France*
[3]*Laboratoire de Physiologie Moléculaire et Cellulaire, UMR 5095 CNRS, Institut de Biochimie et Génétique Cellulaires, 1 rue Camille Saint-Saëns, F-33077 Bordeaux cedex, France*

ATP, the principal energy currency of the cell, fuels most biosynthetic reactions in the cytoplasm by its hydrolysis into ADP and inorganic phosphate. Because resynthesis of ATP occurs in the mitochondrial matrix, ATP is exported into the cytoplasm while ADP is imported into the matrix. The exchange is accomplished by a single protein, the ADP/ATP carrier. Here we have solved the bovine carrier structure at a resolution of 2.2 Å by X-ray crystallography in complex with an inhibitor, carboxyatractyloside. Six α-helices form a compact transmembrane domain, which, at the surface towards the space between inner and outer mitochondrial membranes, reveals a deep depression. At its bottom, a hexapeptide carrying the signature of nucleotide carriers (RRRMMM) is located. Our structure, together with earlier biochemical results, suggests that transport substrates bind to the bottom of the cavity and that translocation results from a transient transition from a 'pit' to a 'channel' conformation.

The transport of various metabolites (nucleotides, phosphate, pyruvate, oxoglutarate, and so on) across the mitochondrial membranes is essential for eukaryotic metabolism. Specific transport through the inner mitochondrial membrane is achieved by nuclear encoded carriers which form a large transport family (the mitochondrial carrier family, MCF)[1]. The exchange of ADP and ATP generates vital energy: each human being exchanges the equivalent of his/her own mass of ATP every day. The regeneration of ATP in mitochondria thus needs an efficient machinery able to import ADP and to export ATP. This transport is achieved by a membrane protein, the ADP/ATP carrier.

Severe diseases such as mitochondrial myopathies or ophthalmoplegia have been associated with dysfunctioning of the human ADP/ATP carrier[2–6]. Translocation is very specifically inhibited by bongkrekic acids, secreted by the bacteria *Pseudomonas cocovenenans*, atractyloside (ATR) and carboxyatractyloside (CATR), of which the last is relevant here. Atractylosides are lethal poisons produced by *Atractylis gummifera*, a Mediterranean thistle known to the ancient Egyptians and described by the Greek physician Dioscorides (~40–90 AD) as a medicinal herb (*Chamaileon Leukos*). More recently ATR and CATR were also identified in other plants[7,8].

The ADP/ATP carrier was discovered four decades ago[9–11] and extensively studied[12,13]. The 297 residues of the bovine carrier have been determined by protein sequencing[14]. It has been proposed that the carriers of various eukaryotic organisms share a high degree of sequence similarity as well as biochemical or functional properties. Human and bovine isoforms 1, localized in cardiac and skeletal muscles, share more than 90% amino acid sequence identity. Yeast and bovine carriers share about 50% identity. All ADP/ATP carriers exhibit a consensus sequence, RRRMMM, that is absent from other mitochondrial carriers. The two families of inhibitors provide tools for characterizing the nucleotide carrier. They were used in fluorescence measurements[15] and in investigation of transport electrogenicity[16]. The results suggest that CATR binding occurs at a site similar to the ADP-binding site, thus preventing ADP/ATP transport.

With respect to the sequence, the carrier was predicted to consist of six transmembrane helices[1]. The hydrophobicity of the second transmembrane helix was found to be rather low[17], and loop protrusions have been suggested[18–20]. Both the amino and carboxy termini were shown to be oriented towards the intermembrane space[21,22]. In functional terms, it was found that, as in most of the carriers, the stoichiometry of exchange of metabolites is one-to-one. The carrier appears to exist in two conformations which are involved in the translocation mechanism: one conformation is stabilized by atractylosides, the second by bongkrekic acid. It is now generally accepted that the functional carrier unit is a dimer. This was deduced from the oligomeric state of the CATR-inhibited carrier, which is a dimer with one CATR per dimer[23,24].

The structures at atomic resolution of several components of oxidative phosphorylation, such as ATP synthase and complexes II–IV of the electron transfer chain have been achieved. More recently, some structures of membrane proteins implicated in transport processes were reported (ion channelling, water or glycerol permeation, transport of small molecules and multidrug efflux) unveiling important mechanistic aspects (for a complete list of membrane protein structures, see http://blanco.biomol.uci.edu/Membrane_Proteins_xtal.html). To provide an insight into the nucleotide transport mechanism, an understanding of the structure of the carrier at high resolution is necessary. We now report this structure, determined by X-ray crystallography, to a resolution of 2.2 Å. Since ADP/ATP carrier is a paradigm for mitochondrial carriers, our results provide the first structural insight into the family of mitochondrial metabolite transporters.

Structure and overall architecture

The crystal unit cell contains one monomer per asymmetric unit and the crystal is packed as protein layers without indication of specific dimerization within the layers. Aminoacyl residues 2 to 293 of the molecule could be located in the model, and in addition, 82 molecules of water, one CATR and four lipids were seen. The transmembrane domain consists of six transmembrane α-helices, all of which are tilted relative to the orthogonal direction of the membrane and to each other (Fig. 1). The six helices form a barrel that defines a deep cone-shaped depression accessible from the

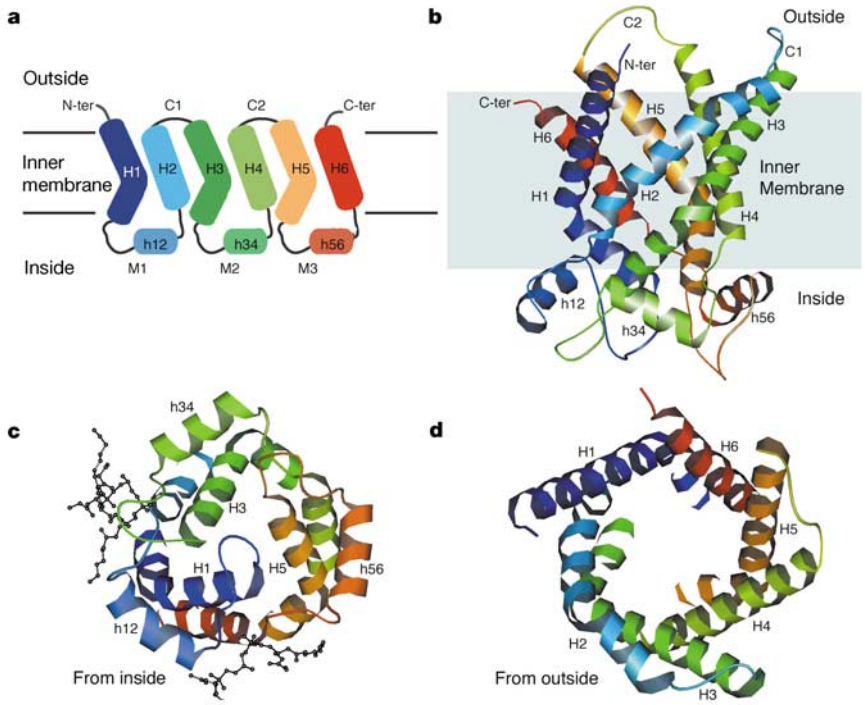

Figure 1 Architecture of the ADP/ATP carrier. **a**, A schematic diagram of the carrier secondary structure. Transmembrane helices, surface helices, intermembrane space loops and matrix loops are labelled H, h, C or M, respectively. Helices comprise the following residues: 4–37 (H1), 53–64 (h12), 73–99 (H2), 108–142 (H3), 156–167 (h34), 176–199 (H4), 209–238 (H5), 253–264 (h56), 273–290 (H6). Odd-numbered helices are kinked by the presence of prolines (P27, P132, P229). Inside and outside designate the matrix and the intermembrane space of mitochondria, respectively. **b**, A ribbon diagram viewing the carrier from the side. The structure is coloured according to the sequence blue (N terminus) to red (C terminus). Membrane boundaries are drawn in agreement with the hydrophobic segments of the helices. **c**, View from the inside. Two cardiolipins are represented in black as ball and sticks. **d**, View from the outside. These and all subsequent ribbon diagrams were drawn with the programs MOLSCRIPT and BOBSCRIPT[49]; surfaces with the program GRASP[50].

outside. The cavity has a maximal diameter of 20 Å and a depth of 30 Å (Fig. 2a). As for all mitochondrial carriers, the gene encoding ADP/ATP carrier presents a threefold duplication that results in a threefold repeat of about 100 amino acids within the protein[17].

Figure 3a shows the alignment of the three repeats, which are related by less than 15% sequence identity. The fold of the three repeats is very similar (Fig. 3b), with root-mean-square deviations on the main chains of less than 2 Å. The connections within pairs of odd- and even-numbered helices contain short α-helical stretches (h12, h34 and h56). Situated parallel to the membrane surface, they appear to strengthen the closed conformation of the carrier on the matrix side (Fig. 1c). The surfaces that are oriented towards the membrane are hydrophobic and possibly interact with the membrane[25]. Each of the odd-numbered helices exhibits a sharp kink, which is due to a proline residue (Fig. 1c and 3b). These prolines are located in the conserved sequence PX(D/E)XX(K/R) characteristic of mitochondrial carriers[1,26]. Exposed on the outside, two short loops connect the three repeats to each other. The structure presents large hydrophilic surfaces, in particular in the interior of the conical pit, explaining the relatively weak hydrophobicity of the transmembrane helices, shown particularly for H2 (ref. 17). The electrostatic potential surface highlights strong positive patches at the bottom of the cavity (Fig. 4a) and weaker positive ones on the matrix side (Fig. 4b). The electron density map, $2F_{obs}–F_{calc}$, as well as the residual map, $F_{obs}–F_{calc}$, reveal cardiolipins in two locations on the matrix side (Fig. 1c), consistent with previous observations describing the presence of a few cardiolipins tightly bound to the carrier[27].

ADP/ATP transport blocked by trapping of CATR in the cavity

The distribution of charges and aromatic residues is asymmetric within the cavity, with a surface near the bottom that is very hydrophilic. Towards the cavity, a cationic cluster consisting of five arginines (R79, R137, R234, R235, R279) and two lysines (K22, K32) points to the solvent. The positions of their side chains are stabilized by an intricate hydrogen-bond network, and by electrostatic interactions involving acidic or polar side chains (E29, D134, D231, Q36, N276 and so on) and water molecules. A second cationic region located near the entrance of the pit comprises residues from helix H2 (K91, K95), loop C1 (R104, K106) and helix H4 (R187, K198). The two basic patches are about 10 Å apart. In the cavity, a tyrosine motif is formed by Y186, Y190 and Y194 located on H4. Their aromatic rings are stacked, pointing with their

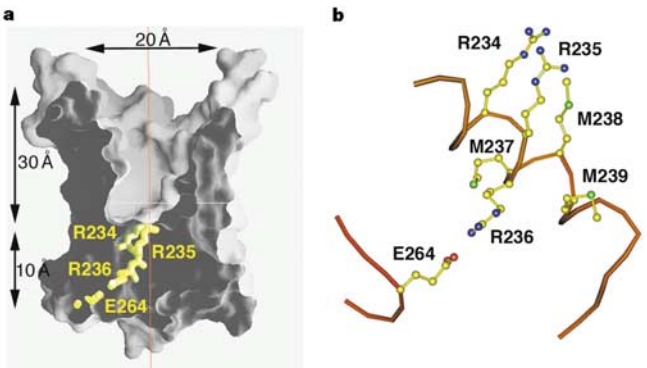

Figure 2 Section through the carrier. At the bottom of the cone-shaped cavity, the hexapeptide (RRMMM signature) can be seen. **a**, The conical pit open to the outside and the RRR sequence spanning through the closed part of the carrier. **b**, A close-up view of the RRRMMM motif in the same orientation.

hydroxyl groups towards the centre of the cavity, thus forming a tyrosine ladder.

Initial experimental electron density maps showed extra density within the pit. After construction and refinement of the peptide chain, a CATR molecule (Fig. 5a–c) could be modelled unambiguously into these maps. CATR is located deeply in the cavity, not centred on the pseudo-threefold axis (Fig. 5b), and trapped through numerous interactions (Fig. 5c, d). The diterpene moiety is inserted towards the matrix side and stacks on the aromatic ring of Y186, while the glucose moiety carrying the two sulphate groups is exposed towards the outside. The tight binding of CATR at the bottom of the cavity is explained by the many hydrogen bonds that, in addition to water molecules, involve most of the basic residues previously mentioned. To determine the importance of the different chemical moieties of CATR, the inhibitory effect of various analogues of CATR have been studied[28].

In our structure, the isovaleric group is in van der Waals contact with hydrophobic side chains (L127, V130, I183). This is consistent with a affinity for ATR of the L142S mutant (equivalent to L127) of *Saccharomyces cerevisiae* ADP/ATP carrier (isoform 2) that is 15 times lower than for the wild type[29]. The sulphate groups are within hydrogen-bond distances of several polar side chains (N87, K91, R187) as well as with the oxygen from the isovaleric residue for one sulphate and the oxygen of the hydroxyl linked to the sugar ring for the second sulphate. The two CATR carboxylic groups interact with the protein. The carboxylate that is common to CATR and ATR forms a salt bridge with R79. The additional carboxylate, characteristic of CATR, interacts with R279 via a water molecule (Fig. 5d), and therefore reinforces the affinity of CATR compared to ATR (the dissociation constant K_d is in the nanomolar range for CATR and is ten times higher for ATR). The primary alcohol group of the glucose moiety can be replaced by various chemical adducts without altering the inhibitory properties. Indeed, this group does not interact with the protein.

In summary, the structure shows that ADP/ATP carrier provides a very tight binding pocket for CATR, explaining the high efficiency of this lethal poison. It also shows why all the chemical groups (except the primary alcohol group of the ribose moiety) present in CATR are important for its toxicity.

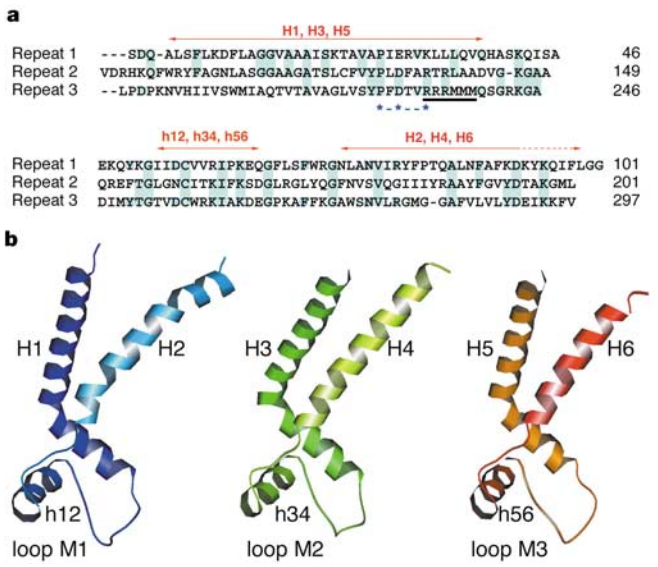

Figure 3 The threefold repeat of the ADP/ATP carrier. **a**, Sequence alignment of the three repeats. Conserved residues are highlighted in blue. Stars indicate the PX(D/E)XX(K/R) sequence. Helices are shown with arrows. The RRRMMM signature of nucleotide carriers is underlined in black. **b**, Structure comparison of the three repeats presented with similar orientations.

Discussion

The physiological role of the carrier is to export ATP from mitochondria in exchange for external ADP. Prior to transport, the carrier has to recognize the nucleotides and in contrast to most of nucleotide-binding proteins, it only binds adenine nucleotides that are not complexed with magnesium ions. Consensus nucleotide binding sequences such as Walker motifs are not present in the carrier. The ADP/ATP carrier is thought to function as a dimer that works as an antiport. Indeed, ADP/ATP transport has been demonstrated on kinetic grounds to proceed with a sequential mechanism accounting for the one-to-one stoichiometry of the exchange[30]. In the absence of nucleotides, the carrier is thought to be multiconformational. Each monomer within the dimer has two favourable conformations that can bind ADP or ATP from the outside or from the inside, respectively. Transport takes place once ADP binds to one monomer from the outside and ATP to the second monomer from the inside, simultaneously.

This antiport model resulting from various biochemical data raises several questions. What are the structural elements or amino acids involved in the nucleotide binding from each side? How flexible must the protein be to achieve the conformational changes associated with nucleotide binding and to allow the antiport process to take place? How are these changes triggered? We now discuss these questions in the light of our structure.

Structural basis for nucleotide binding

CATR binding is exclusive to nucleotide binding, raising the question of whether the binding sites are the same. Several genetic and biochemical approaches have aimed at identifying the residues that are important for nucleotide binding. In the *S. cerevisiae* carrier, the R96H mutation (named *op1*) drastically diminishes ADP binding affinity[31,32]. Therefore, the bovine R79 residue (R96 in yeast) is most probably implicated in the binding of ADP. All the basic residues located at the bottom of the cavity in the bovine protein are highly conserved and therefore participate putatively in the binding of the negatively charged nucleotides. Indeed the role of many basic residues of the yeast carrier was investigated by mutagenesis. Arginines 96 (79), 204 (187), 252 (234), 253 (235), or 294 (279) as well as lysine 38 (22) (the corresponding residues of the bovine carrier are in parentheses) were shown to be essential for the transport activity[33], in contrast to K179 (162) and K182 (165) that can be mutated concomitantly into isoleucines without affecting the function[34].

In our structure, the residues shown to be important for the activity are interacting with CATR and are located within the putative nucleotide-binding site. By analogy to the van der Waals distance between the diterpene moiety of CATR and Y186, the adenine ring could interact with Y186, a highly conserved residue within the ADP/ATP carrier family. Similar types of interactions

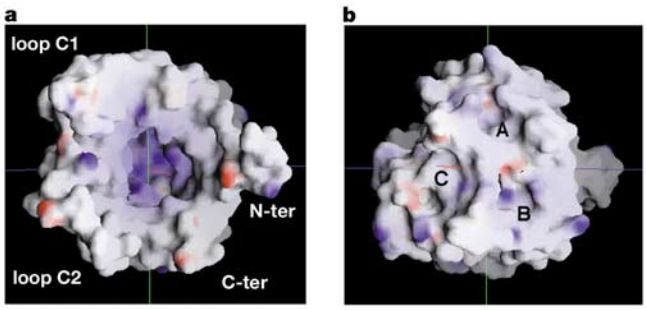

Figure 4 Electrostatic potential surface. Positive and negative surfaces are shown in blue and red, respectively. **a**, View from the outside. **b**, View from the inside showing three small cavities (A, B, C). Two cationic patches are located in the regions labelled B (R139/K162/K165) and C (R236/R243/R258/K259).

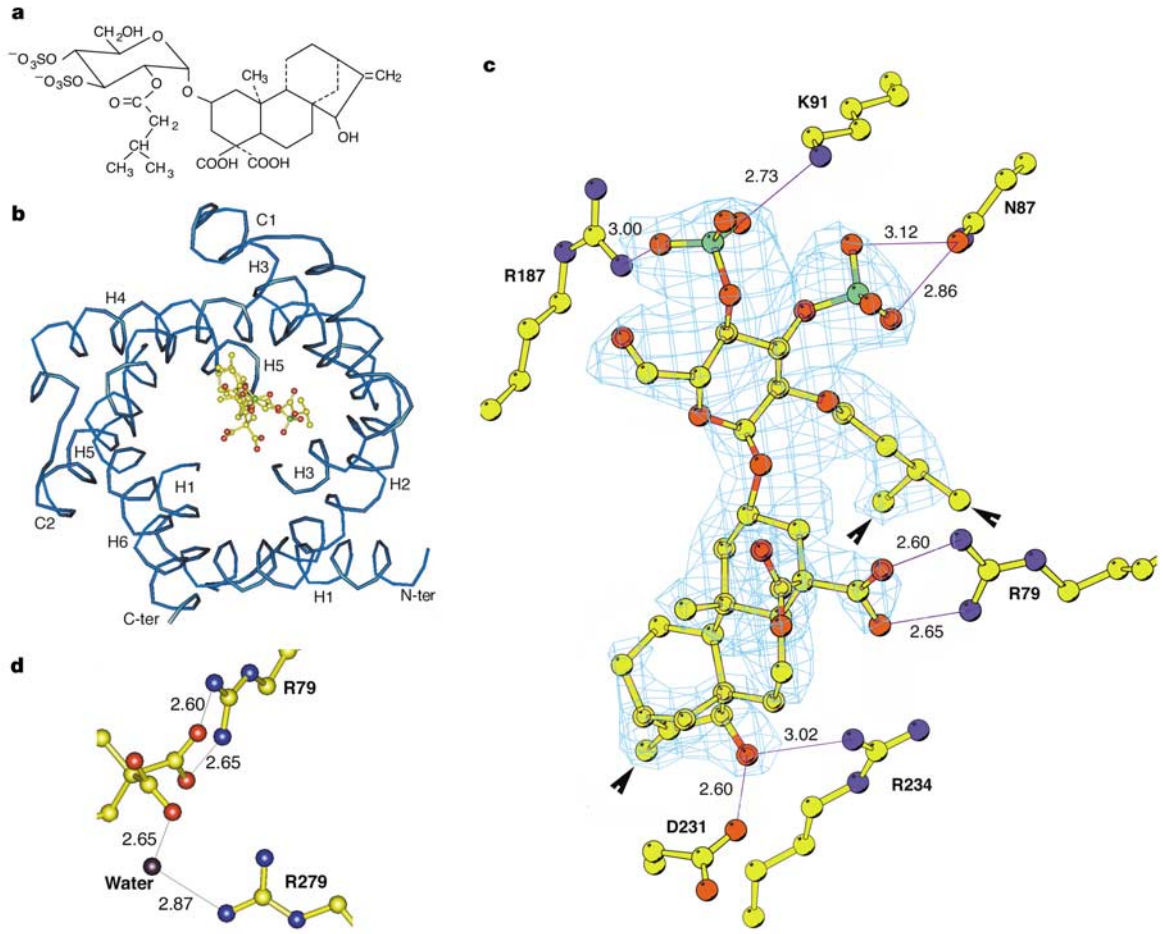

Figure 5 The binding of CATR. **a**, Chemical formula of CATR. **b**, CATR within the binding pocket viewed from the outside. **c**, Electron density map at 2.2 Å resolution ($2F_{obs} - F_{calc}$, contoured at 1σ obtained before CATR modelling and including only protein atoms) around CATR. Residues directly within hydrogen-bond distances to CATR are labelled. Black arrowheads indicate van der Waals contacts between CATR and the protein. **d**, A close-up of the two CATR carboxylates interacting with arginines. Interatomic distances are given in Å.

were observed in the structures of several ATP-binding proteins[35]. Altogether, these facts support the idea that ADP and CATR binding sites overlap. In addition, structural features hint how nucleotides could be guided towards the binding site. The patch of basic residues described at the entrance of the surmised channel could participate in attracting nucleotides towards their binding site. A stacking interaction with tyrosine rings could guide the ADP translocation along the tyrosine ladder (Y186, Y190, Y194). In yeast, we have shown that double mutations of Y203 and Y207 (equivalent to Y186 and Y190 in the bovine carrier) prevented or slightly reduced cellular growth on a non-fermentable carbon source when mutated into alanines or phenylalanines, respectively (data not shown).

RRRMMM may trigger conformational change

The conformation of the carrier required for ATP binding from the matrix is probably different from the ADP-binding conformation and therefore, assessment of the ATP binding site is more speculative. Individual mutations of arginines in the RRRMMM motif abolish the transport activity. The three arginines span over the apparent barrier, depicted in Fig. 2a, that the nucleotide has to cross during translocation through the membrane. R234 and R235 are implicated in CATR binding and therefore possibly in ADP binding. R236, which points in the opposite direction (Fig. 2b), forms a salt bridge with E264 (also conserved among the nucleotide carriers), contributing to the interaction of M3 with the core of the protein. Matrix loop M3 contains a sequence of eight amino acids including charged amino acids E264, K267 and K271. It was reported that Asp or Glu carboxylates are possible partners in hydrogen bonds with adenine or ribose moieties, while lysine Nζ nitrogens interact frequently with phosphate oxygens[35,36]. The salt bridge involving E264 with R236 hides both side chains from the surface, impairing potential nucleotide binding. On the basis of the structure, we propose RRR to be a two-way switch that dictates nucleotide binding stoichiometry. ATP coming from the matrix might destabilize the salt bridge, inducing a local rearrangement of the RRR structure due to the reorientation of E264 and thus impeding the accessibility of R234 and R235 to external nucleotides. Conversely, binding of ADP from the outside would mask R236 and prevent nucleotide binding from the matrix. In the structure MMM occupies a bulky volume (Fig. 2b) that could control the access, acting as a plug during the transport mechanism. In addition, a possible reorientation of E264 that favoured ATP interaction with the glutamate via its adenine or ribose moiety could also favour ATP interaction with K267 or K271 via the phosphate groups.

Hinges and channel opening

Figure 6 depicts the conformation of odd-numbered helices and shows how the prolines of the PX(D/E)XX(K/R) sequence impose a kink on them. Three pairs of charged residues strengthen a closed conformation by multiple interactions. We propose that during the transport process prolines act as hinges that would straighten odd-

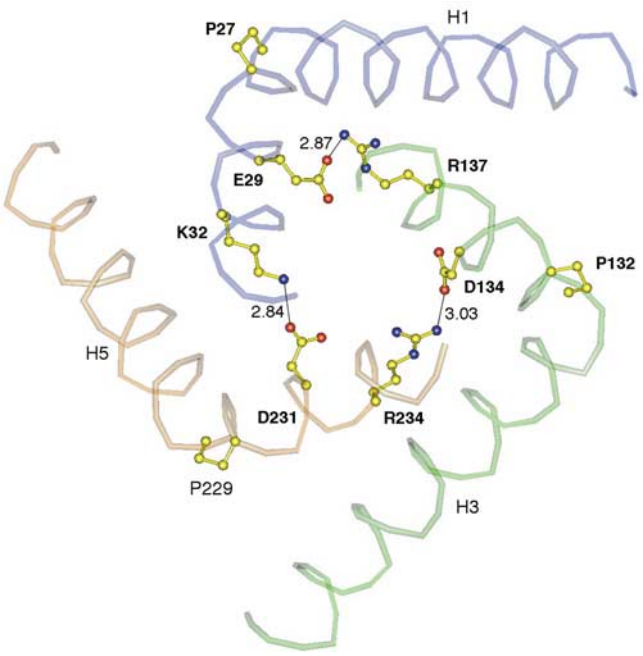

Figure 6 The closed conformation of the carrier viewed from the matrix. Only odd-numbered helices are represented. Residues involved in the PX(D/E)XX(K/R) sequence are labelled. Black lines connect atoms within hydrogen-bonding distances (in Å).

numbered helices, thus reshaping the protein and pulling open a channel. This would also imply a reorganization of charged pairs (Fig. 6) as previously suggested[26]. Opening and closing channels through helix bending was also proposed for other proteins[37,38]. Once channels are formed, the vectoriality of the transport within the ADP/ATP carrier is probably guided by the electrostatic environment.

To prevent binding of two nucleotides from the same side on each monomer within a dimer, we postulate that dimeric structural constraints require the conformations of both monomers to be out-of-phase. Therefore, binding of one nucleotide from either side of the carrier favours binding of a second one from the opposite side, consistent with previously reported biochemical data[39]. Simultaneous binding of both nucleotides could impose lateral forces on odd-numbered helices, modifying their bending as described above. Many features of the structure disrupt the threefold symmetry of the carrier monomer structure. In particular, M1 is connected to the core of the protein through a number of hydrogen-bonding and electrostatic interactions that is significantly larger than for M2 or M3. These observations raise the question of whether the three matrix loops follow a symmetric movement during the transport.

Conclusion

The structure of the ADP/ATP carrier complexed with CATR provides an insight into one conformation of the protein. It provides the molecular basis of the high-affinity binding of CATR and excludes CATR binding between two monomers, as previously proposed. Even though the structure that we describe here represents a monomer, key structural determinants that are important in nucleotide transport can be learned from it. RRRMMM, the ADP/ATP carrier signature, spans over the thinnest part of the protein in a strategic location for the transport. Attraction of ADP towards the matrix against the natural electrostatic potential is highlighted by the distribution of positive charge patches within the protein cavity. The carrier has a closed conformation on the matrix side induced by kinks in odd-numbered helices due to the presence of prolines. We hypothesize that the transport itself could be triggered by cooperative binding of nucleotides and achieved through channels that open as the odd-numbered transmembrane helices un-tilt with respect to the membrane, with the prolines acting as hinges. To sustain this hypothesis the different conformations have to be explored by various methods including two-dimensional electron microscopy[40] or X-ray crystallography. Because the PX(D/E)XX(K/R) sequence is characteristic of all mitochondrial carriers, the opening mechanism could be extended to other transporters, the transition from open to closed states being specifically triggered by the binding of transported metabolites.

It is also probable that ADP/ATP transport in mitochondria cannot be described fully at the molecular level only: it may well result from a combination of stochastic events and parameters of the local environment, including membrane potential and nucleotide concentrations on both sides of the inner membrane. Although our model sheds light on some features of the mechanism, the nucleotide selectivity (adenine versus guanine), the transport itself once nucleotides are bound, and kinetic aspects need additional experimental investigations to be deciphered. □

Methods

Detailed information on methodological aspects is provided as Supplementary Information.

Purification and crystallization

The ADP/ATP carrier (relative molecular mass, $M_w = 33{,}000$ for the monomer) was isolated from beef heart mitochondria as a CATR-carrier complex in the presence of the detergent 3-laurylamido-N,N′-dimethylpropylaminoxide (LAPAO) according to the procedure of ref. 24 with minor modifications. The purified carrier fraction was treated with Bio-Beads (BioRad) to remove excess detergent[41] before concentration. Crystals were grown by hanging-drop vapour diffusion at 20 °C by mixing equal volumes of protein and reservoir. Two different orthorhombic crystal forms were obtained in the presence of 30% Jeffamine-M600 (O-(2-aminopropyl)-O′-(2-methoxyethyl)polypropylene glycol 500) as a precipitant. The first crystals are primitive ($P2_12_12$, $a = 85.4$ Å, $b = 83.5$ Å, $c = 49.9$ Å) and the second ones centred ($C222_1$, $a = 79.9$ Å, $b = 109.2$ Å, $c = 89.3$ Å). The primitive crystal form used for the refinement contains monomers probably due to selective crystallization of the CATR-carrier monomeric complex. Excessive delipidation could account for dimer dissociation. Indeed, it was reported that lipids contribute strongly to oligomerization as shown in bacteriorhodopsin[42] or bacterial cytochrome *c* oxidase[43].

Structure determination

Numerous data sets were collected at the European Synchrotron Radiation Facility, Grenoble (ESRF), on beam lines BM30A, ID14-1, ID14-2 and ID29, at 100 K under nitrogen stream. Data sets used for phasing and refinement were collected on beamlines ID29 and BM30A. All data sets were processed with DENZO, SCALEPACK[44] and CCP4[45]. Most of the primitive crystals presented a defect and were not usable, with the exception of one good native data set to 2.2 Å that was used for the model refinement. The heavy-atom derivatives necessary for the phase determination were screened with the centred form despite anisotropic diffraction. Three mercury derivatives were collected and used in phase determination with phasing powers of 1.80, 1.58 and 1.70, respectively. Heavy-atom site positions deduced manually from Patterson maps were refined and phases calculated using MLPHARE[45]. Initial phases were improved by solvent flattening using DM[45], increasing the figure of merit from 0.55 to 0.69. The model was built using O[46] and refinement was carried out using CNS[47]. The electron density map clearly showed six helices. A first model containing the helices and part of the loops was constructed in the centred crystal form and transposed to the primitive form by molecular replacement[48]. The model construction was improved using both the experimental electron density transposed to the primitive crystal form according to the rotation matrix and translation vector obtained by molecular replacement and the $2F_{obs} - F_{calc}$ maps. The model was refined by iterative cycles of manual corrections and energy minimization or simulated annealing followed by individual *B*-factor refinements, to a final R_{cryst} of 22.6% and R_{free} of 26.8% to 2.2 Å resolution.

Received 27 June; accepted 15 September 2003; doi:10.1038/nature02056.

1. Walker, J. E. & Runswick, M. J. The mitochondrial transport protein superfamily. *J. Bioenerg. Biomembr.* **25,** 435–446 (1993).
2. Torroni, A., Stepien, G., Hodge, J. A. & Wallace, D. C. Neoplastic transformation is associated with coordinate induction of nuclear and cytoplasmic oxidative phosphorylation genes. *J. Biol. Chem.* **265,** 20589–20593 (1990).
3. Heddi, A., Lestienne, P., Wallace, D. C. & Stepien, G. Mitochondrial DNA expression in mitochondrial myopathies and coordinated expression of nuclear genes involved in ATP production. *J. Biol. Chem.* **268,** 12156–12163 (1993).
4. Kaukonen, J. *et al.* Role of adenine nucleotide translocator 1 in mtDNA maintenance. *Science* **289,** 782–785 (2000).
5. Fiore, C., Arlot-Guilligay, D., Trézéguet, V., Lauquin, G. J. & Brandolin, G. Fluorometric detection of ADP/ATP carrier deficiency in human muscle. *Clin. Chim. Acta* **311,** 125–135 (2001).
6. Napoli, L. *et al.* A novel missense adenine nucleotide translocator-1 gene mutation in a Greek adPEO family. *Neurology* **57,** 2295–2298 (2001).

7. Craig, J. C., Mole, M., Billets, S. & El-Feraly, F. Isolation and identification of hypoglycemic agent carboxyatractylate from *Xanthium strumarium*. *Phytochemistry* **15,** 1178 (1976).
8. Candy, H. A., Pegel, K. H., Brookes, B. & Rodwell, M. The occurrence of atractyloside in *Callilepsis laureola*. *Phytochemistry* **16,** 1308–1309 (1977).
9. Bruni, A., Luciani, S. & Contessa, A. R. Inhibition by atractyloside of the binding of adenine nucleotides of rat liver mitochondria. *Nature* **201,** 1219–1220 (1964).
10. Duée, E. D. & Vignais, P. V. Exchange between extra- and intramitochondrial adenine nucleotides. *Biochim. Biophys. Acta* **107,** 184–188 (1965).
11. Pfaff, E., Klingenberg, M. & Heldt, H. W. Unspecific permeation and specific exchange of adenine nucleotides in liver mitochondria. *Biochim. Biophys. Acta* **104,** 312–315 (1965).
12. Klingenberg, M. Molecular aspects of the adenine nucleotide carrier from mitochondria. *Arch. Biochem. Biophys.* **270,** 1–14 (1989).
13. Fiore, C. *et al.* The mitochondrial ADP/ATP carrier: structural, physiological and pathological aspects. *Biochimie* **80,** 137–150 (1998).
14. Aquila, H., Misra, D., Eulitz, M. & Klingenberg, M. Complete aminoacid sequence of the ADP/ATP carrier from beef heart mitochondria. *Hoppe-Seyler's J. Physiol. Chem.* **363,** 345–349 (1982).
15. Brandolin, G., Dupont, Y. & Vignais, P. V. Substrate-induced modifications of the intrinsic fluorescence of the isolated adenine nucleotide carrier protein: demonstration of distinct conformational states. *Biochemistry* **24,** 1991–1997 (1985).
16. Gropp, T. *et al.* Kinetics of electrogenic transport by the ADP/ATP carrier. *Biophys. J.* **77,** 714–726 (1999).
17. Walker, J. E. The mitochondrial transporter family. *Curr. Opin. Struct. Biol.* **2,** 519–526 (1992).
18. Bogner, W., Aquila, H. & Klingenberg, M. The transmembrane arrangement of the ADP/ATP carrier as elucidated by the lysine reagent pyridoxal 5-phosphate. *Eur. J. Biochem.* **161,** 611–620 (1986).
19. Majima, E., Koike, H., Hong, Y. M., Shinohara, Y. & Terada, H. Characterization of cysteine residues of mitochondrial ADP/ATP carrier with the SH-reagents eosin 5-maleimide and N-ethylmaleimide. *J. Biol. Chem.* **268,** 22181–22187 (1993).
20. Dianoux, A. C. *et al.* Two distinct regions of the yeast mitochondrial ADP/ATP carrier are photolabeled by a new ADP analogue: 2-azido-3′-O-naphthoyl-[β-^{32}P]ADP. Identification of the binding segments by mass spectrometry. *Biochemistry* **39,** 11477–11487 (2000).
21. Brandolin, G., Boulay, F., Dalbon, P. & Vignais, P. V. Orientation of the N-terminal region of the membrane-bound ADP/ATP carrier protein explored by antipeptide antibodies and an arginine-specific endoprotease. Evidence that the accessibility of the N-terminal residues depends on the conformational state of the carrier. *Biochemistry* **28,** 1093–1100 (1989).
22. Trézéguet, V. *et al.* A covalent tandem dimer of the mitochondrial ADP/ATP carrier is functional *in vivo*. *Biochim. Biophys. Acta* **1457,** 81–93 (2000).
23. Hackenberg, H. & Klingenberg, M. Molecular weight and hydrodynamic parameters of the adenosine 5′-diphosphate/adenosine 5′-triphosphate carrier in TritonX-100. *Biochemistry* **19,** 548–555 (1980).
24. Block, M. R., Zaccai, G., Lauquin, G. J. & Vignais, P. V. Small angle neutron scattering of the mitochondrial ADP/ATP carrier protein in detergent. *Biochem. Biophys. Res. Commun.* **109,** 471–477 (1982).
25. Panneels, V., Schussler, U., Costagliola, S. & Sinning, I. Choline head groups stabilize the matrix loop regions of the ATP/ADP carrier ScAAC2. *Biochem. Biophys. Res. Commun.* **300,** 65–74 (2003).
26. Nelson, D. R., Felix, C. M. & Swanson, J. M. Highly conserved charge-pair networks in the mitochondrial carrier family. *J. Mol. Biol.* **277,** 285–308 (1998).
27. Beyer, K. & Klingenberg, M. ADP/ATP carrier protein from beef heart mitochondria has high amounts of tightly bound cardiolipin, as revealed by ^{31}P nuclear magnetic resonance. *Biochemistry* **24,** 3821–3826 (1985).
28. Vignais, P. V. Molecular and physiological aspects of adenine nucleotide transport in mitochondria. *Biochim. Biophys. Acta* **456,** 1–38 (1976).
29. Zeman, I. *et al.* Four mutations in transmembrane domains of the mitochondrial ADP/ATP carrier increase resistance to bongkrekic acid. *J. Bioenerg. Biomembr.* **35,** 243–256 (2003).
30. Duyckaerts, C., Sluse-Goffart, C. M., Fux, J. P., Sluse, F. E. & Liebecq, C. Kinetic mechanism of the exchanges catalysed by the adenine-nucleotide carrier. *Eur. J. Biochem.* **106,** 1–6 (1980).
31. Kovac, L., Lachowicz, T. M. & Slonimski, P. P. Biochemical genetics of oxidative phosphorylation. *Science* **158,** 1564–1567 (1967).
32. Beck, J. C., Mattoon, J. R., Hawthorne, D. C. & Sherman, F. Genetic modification of energy-conserving systems in yeast mitochondria. *Proc. Natl Acad. Sci. USA* **60,** 186–193 (1968).
33. Nelson, D. R., Lawson, J. E., Klingenberg, M. & Douglas, M. G. Site-directed mutagenesis of the yeast mitochondrial ADP/ATP translocator. Six arginines and one lysine are essential. *J. Mol. Biol.* **230,** 1159–1170 (1993).
34. Müller, V., Heidkamper, D., Nelson, D. R. & Klingenberg, M. Mutagenesis of some positive and negative residues occurring in repeat triad residues in the ADP/ATP carrier from yeast. *Biochemistry* **36,** 16008–16018 (1997).
35. Denessiouk, K. A. & Johnson, M. S. When fold is not important: a common structural framework for adenine and AMP binding in 12 unrelated protein families. *Proteins* **38,** 310–326 (2000).
36. Moodie, S. L., Mitchell, J. B. & Thornton, J. M. Protein recognition of adenylate: an example of a fuzzy recognition template. *J. Mol. Biol.* **263,** 486–500 (1996).
37. Jiang, Y. *et al.* Crystal structure and mechanism of a calcium-gated potassium channel. *Nature* **417,** 515–522 (2002).
38. Abramson, J. *et al.* Structure and mechanism of the lactose permease of *Escherichia coli*. *Science* **301,** 610–615 (2003).
39. Block, M. R. & Vignais, P. V. Substrate-site interactions in the membrane-bound adenine-nucleotide carrier as disclosed by ADP and ATP analogs. *Biochim. Biophys. Acta* **767,** 369–376 (1984).
40. Kunji, E. R. & Harding, M. Projection structure of the atractyloside-inhibited mitochondrial ADP/ATP carrier of *Saccharomyces cerevisiae*. *J. Biol. Chem.* **278,** 36985–36988 (2003).
41. Holloway, P. W. A simple procedure for removal of Triton X-100 from protein samples. *Anal. Biochem.* **53,** 304–308 (1973).
42. Belrhali, H. *et al.* Protein, lipid and water organization in bacteriorhodopsin crystals: a molecular view of the purple membrane at 1.9 Å resolution. *Struct. Fold. Des.* **7,** 909–917 (1999).
43. Harrenga, A. & Michel, H. The cytochrome c oxidase from *Paracoccus denitrificans* does not change the metal center ligation upon reduction. *J. Biol. Chem.* **274,** 33296–33299 (1999).
44. Otwinowski, Z. & Minor, W. Processing of X-ray diffraction data collected in oscillation mode. *Methods Enzymol.* **276,** 307–326 (1997).
45. The CCP4 suite: programs for X-ray crystallography. *Acta Crystallogr. D* **50,** 760–763 (1994).
46. Jones, T. A., Zou, J. Y., Cowan, S. W. & Kjeldgaard, M. Improved methods for building protein models in electron density maps and the location of errors in these models. *Acta Crystallogr. A* **47,** 110–119 (1991).
47. Brunger, A. T. *et al.* Crystallography & NMR system: A new software suite for macromolecular structure determination. *Acta Crystallogr. D* **54,** 905–921 (1998).
48. Navaza, J. Implementation of molecular replacement in AMoRe. *Acta Crystallogr. D* **57,** 1367–1372 (2001).
49. Esnouf, R. M. Further additions to MolScript version 1.4, including reading and contouring of electron-density maps. *Acta Crystallogr. D* **55,** 938–940 (1999).
50. Nicholls, A., Sharp, K. A. & Honig, B. Protein folding and association: insights from the interfacial and thermodynamic properties of hydrocarbons. *Proteins* **11,** 281–296 (1991).

Supplementary Information accompanies the paper on **www.nature.com/nature**.

Acknowledgements We thank the staff at the European Synchrotron Radiation Facilities and of the French beamline BM30A (ESRF) for synchrotron support. We also thank J. P. Rosenbusch and R. Douce for reading the manuscript, and for numerous suggestions and discussions, and P. V. Vignais for helpful comments. This work was supported by the programmes PCV (CNRS) and Emergence (Région Rhône-Alpes) and by the Région Aquitaine.

Competing interests statement The authors declare that they have no competing financial interests.

Correspondence and requests for materials should be addressed to E.P.P. (pebay@ibs.fr) or G.B. (gbrandolin@cea.fr). Coordinates have been deposited in the Protein Data Bank under accession code 1okc.